International Journal of Control
Publication details, including instructions for authors and subscription information:
http://www.informaworld.com/smpp/title~content=t713393989

L_1 adaptive controller for tailless unstable aircraft in the presence of unknown actuator failures

Vijay V. Patel [a]; Chengyu Cao [b]; Naira Hovakimyan [c]; Kevin A. Wise [d]; Eugene Lavretsky [d]
[a] Department of Aerospace & Ocean Engineering, Virginia Polytechnic Institute & State University, Blacksburg, VA, USA [b] Department of Mechanical Engineering, University of Connecticut, Storrs, USA [c] Department of Mechanical Science and Engineering, University of Illinois at Urbana-Champaign, Urbana, USA [d] Boeing Co., Huntington Beach, USA

First Published:April2009

To cite this Article Patel, Vijay V., Cao, Chengyu, Hovakimyan, Naira, Wise, Kevin A. and Lavretsky, Eugene(2009)'L_1 adaptive controller for tailless unstable aircraft in the presence of unknown actuator failures',International Journal of Control,82:4,705 — 720
To link to this Article: DOI: 10.1080/00207170802225955
URL: http://dx.doi.org/10.1080/00207170802225955

International Journal of Control
Vol. 82, No. 4, April 2009, 705–720

Taylor & Francis
Taylor & Francis Group

$\mathcal{L}_1$ adaptive controller for tailless unstable aircraft in the presence of unknown actuator failures

Vijay V. Patel[a], Chengyu Cao[b]*, Naira Hovakimyan[c], Kevin A. Wise[d] and Eugene Lavretsky[d]

[a]*Department of Aerospace & Ocean Engineering, Virginia Polytechnic Institute & State University, Blacksburg, VA, USA;* [b]*Department of Mechanical Engineering, University of Connecticut, Storrs, USA;* [c]*Department of Mechanical Science and Engineering, University of Illinois at Urbana-Champaign, Urbana, USA;* [d]*Boeing Co., Huntington Beach, USA*

(*Received 18 February 2008; final version received 22 May 2008*)

This article considers application of $\mathcal{L}_1$ adaptive controller to multi-input multi-output open loop unstable unmanned military aircraft. The control is designed to accommodate and to be robust to actuator failures as well as to pitch break uncertainty, which is used to model uncertain aerodynamics. Results of using the $\mathcal{L}_1$ adaptive controller are compared with the conventional model reference adaptive control scheme to show improved transient command tracking as well as *guaranteed* time-delay margin.

Keywords: adaptive control; transient performance; guaranteed time-delay margin; flight control

1. Introduction

Since the early 1990s, the Air Force, Navy and NASA working with industry and academia have made significant progress towards maturing adaptive control theory for application to reconfigurable/damage adaptive flight control for aircraft and weapons systems (McFarland and Calise 1996, 1997; Kim and Calise 1997; Ward 1998; Wise and Brinker 1998; Urnes 1999; Wise et al. 1999; Brinker and Wise 2000; Sharma, Calise and Corban 2000; Sharma and Calise 2001; Corban et al. 2002; Lavretsky and Hovakimyan 2004; Sharma, Wise and Lavretsky 2006). Reconfigurable flight control refers to the ability of a flight control system to adapt to unknown failures, damage and uncertain aerodynamics. Flight control systems that are reconfigurable and adaptive constitute an important element in the design of mission-effective unmanned combat systems. Moreover, these architectures play an important role in increasing the reliability of unmanned systems. Both indirect and direct adaptive control methods have been investigated, and several different approaches have been successfully flown on manned aircraft (Kim and Calise 1997; Ward 1998; Urnes 1999), unmanned aircraft (Wise and Brinker 1998; Wise et al. 1999) and also on advanced weapon systems (Sharma et al. 2000; Sharma and Calise 2001; Corban et al. 2002).

The Self Designing Controller (Ward 1998) program successfully flight tested an indirect adaptive scheme on the VISTA/F-16 aircraft, which used least squares system identification, with spatial and temporal constraints, to estimate the stability and control derivatives required for the solution of a receding horizon optimal control problem. NASA (Urnes 1999) has also tested both an indirect and direct adaptive method on an F-15 aircraft. The indirect method used neural network (NN)-based system identification algorithms to estimate aircraft plant matrices (A, B), and fed these to an online Riccati equation solver. Kim and Calise (1997) presented an approach based on NNs for a feedback linearisation control architecture and demonstrated the approach via simulation studies with an F/A-18 aircraft. This approach was later modified and used in the Reconfigurable Control for Tailless Fighters (RESTORE) programme (Kim and Calise 1997; Wise and Brinker 1998; Wise et al. 1999), using a dynamic inversion control law in an explicit model following framework. The successful application of this technology under the RESTORE program (Wise et al. 1999) led to the flight testing of the approach on the Boeing/NASA X-36 Agility Research Test Aircraft. NASA has also been flight testing a similar approach on their F-15 aircraft. This same approach also has been applied and flown on the Joint Direct Attack Munition (JDAM) (Sharma et al. 2000, 2006; Corban et al. 2002; Wise et al. 2005), in which the LQR-based flight control system was replaced with a dynamic inversion-based scheme augmented with a NN-based model reference adaptive control. A historical overview of research on reconfigurable flight control is available in Steinberg (2005).

Lavretsky and Wise (2005) applied model reference adaptive control (MRAC) to a model of the

*Corresponding author. Email: ccao@engr.uconn.edu

ISSN 0020–7179 print/ISSN 1366–5820 online

DOI: 10.1080/00207170802225955
http://www.informaworld.com

aerodynamically unstable X-45A UCAV. Although successful, implementation of the adaptive control proved to be sensitive to the size of the learning rate, requiring numerical simulations to validate robustness to time-delays. Other open problems regarding the application of MRAC control to aircraft have been documented in Wise, Lavretsky and Hovakimyan (2006).

This article presents application of $\mathcal{L}_1$ adaptive controller to the unmanned military aircraft model from Lavretsky and Wise (2005). The $\mathcal{L}_1$ adaptive controller was first introduced in Cao and Hovakimyan (2006a,b,c) for linear and non-linear systems with known high-frequency gain, and later extended to systems of unknown high-frequency gain, with time-varying parameters and disturbances, in Cao and Hovakimyan (2007a). In Cao and Hovakimyan (2007b), it was proven to have guaranteed time-delay margin in the presence of fast adaptation. In this article, we extend the methodology from Cao and Hovakimyan (2006c) to multi-input multi-output systems of unknown high-frequency gain using the basic architecture from Cao and Hovakimyan (2007b). From that perspective, this article presents an extension of the earlier results from Patel, Cao, Hovakimyan, Wise and Lavretsky (2007), where no actuator failures have been included in the model.

In Lavretsky and Wise (2005) the adaptive control architecture includes a baseline inner-loop control, which is augmented by an online feedforward NN. The baseline inner loop control provides nominal system performance, while the adaptive increment accommodates unknown/unexpected control failures and model uncertainties. The approach in this article presents application of $\mathcal{L}_1$ adaptive controller to the unstable X-45A UCAV model in the presence of actuator failures and pitch break uncertainty (unknown non-linear in Angle of Attack (AOA) pitching moment increment). This uncertainty is introduced in pitch dynamics in order to model unknown changes in the aircraft pitching moment that can drive the aircraft into an uncontrollable (in AOA) region. The benefit of $\mathcal{L}_1$ adaptive controller is its capacity for fast and robust adaptation that leads to desired transient performance for both system's signals, input and output, simultaneously. Moreover, for systems linearly dependent upon unknown parameters, the (non-linear) $\mathcal{L}_1$ adaptive controller has analytically computable and guaranteed time-delay margin. From that perspective, the $\mathcal{L}_1$ adaptive control architecture provides a solution to one of the open problems stated in Wise et al. (2006). In the case of non-linear systems, as the one considered in this article, the margins are computed numerically based on simulations. However, the insights are based on the theoretical analysis of the linear systems, which provides guidelines as how to choose the underlying filter for maximising the time-delay margin (Cao and Hovakimyan 2007b). An excellent discussion on phase margin and its relation to time-delay margin for four different control architectures with emphasis on high gain versus fast dynamics and adaptive versus non-adaptive scheme can be found in Cao et al. (2006).

The article is organised as follows. Section 2 gives the problem formulation. In § 3, the novel $\mathcal{L}_1$ adaptive control architecture is presented. Stability and uniform transient tracking bounds of the $\mathcal{L}_1$ adaptive controller are presented in § 4. In § 5, simulation results are presented, while § 6 concludes the article.

2. Problem formulation

Following Lavretsky and Wise (2005) we present aircraft dynamics as

$$\begin{aligned} &\dot{x}(t) = Ax(t) + B_1\Lambda\big(\delta(t) + K_0(x_p(t))\big) + B_2u(t)\,,\\ &x(0) = x_0 = 0\,, \end{aligned} \tag{1}$$

where $x(t)\in\mathbb{R}^9$, $\delta(t)\in\mathbb{R}^3$ (virtual control input), $u(t)\in\mathbb{R}^4$ are the measured system states, control signals and reference inputs, respectively, $A\in\mathbb{R}^{9\times9}$, $B_2\in\mathbb{R}^{9\times4}$, $B_1\in\mathbb{R}^{9\times3}$ are known matrices where the three columns of B_1 are linearly independent, and

$$\Lambda = \begin{bmatrix} \Lambda_1 & 0 & 0\\ 0 & \Lambda_2 & 0\\ 0 & 0 & \Lambda_3 \end{bmatrix} \tag{2}$$

is an unknown diagonal matrix with strictly positive diagonal elements. The state vector $x=(\alpha,\beta,p,q,r,q_I,p_I,r_I,r_w)^\top$ comprises five plant states (x_p), which include angle of attack α, angle of sideslip β, body roll rate p, body pitch rate q, body yaw rate r and four baseline controller (x_c) states, which include pitch, roll and yaw (q_I, p_I and r_I) integrator states and yaw rate washout filter signal r_w. The vector $u=(a_z^{cmd},\beta^{cmd},p^{cmd},r^{cmd})^\top$ consists of four inner loop commands that include vertical acceleration, sideslip, roll rate and yaw rate, while δ is the vector of virtual controls (roll, pitch and yaw control). Our control design relies on the following assumptions.

Assumption 1:

$$\Lambda_i \in [\Lambda_l,\ \Lambda_u], \tag{3}$$

where $\Lambda_u > \Lambda_l > 0$ are known.

Assumption 2:

$$\|K_0(0)\|_\infty \le B\,, \tag{4}$$

where $B>0$ is a known conservative bound.

Assumption 3: *A conservative Lipschitz constant* $L_w > 0$ *is known such that*

$$\|\Lambda(K_0(x_{p1}) - K_0(x_{p2}))\|_\infty \leq L_w \|x_{p1} - x_{p2}\|_\infty. \quad (5)$$

Since

$$\|x_{p1} - x_{p2}\|_\infty \leq \|x_1 - x_2\|_\infty, \quad (6)$$

we can write (5) in the form:

$$\|\Lambda(K_0(x_{p1}) - K_0(x_{p2}))\|_\infty \leq L_w \|x_1 - x_2\|_\infty. \quad (7)$$

Note that the vector-function $K_0(x_p)$ represents matched unknown non-linearities. In addition to unknown $K_0(x_p)$, Λ models actuator failures and loss of control effectiveness. The inner-loop control objective is to design a full state-feedback controller $\delta(t)$ for (1) such that all closed-loop signals remain bounded, and the system state tracks the state of a desired reference model.

3. $\mathcal{L}_1$ adaptive controller

Consider the following control law:

$$\delta(t) = \delta_{\mathrm{L}}(t) + \delta_{\mathrm{ad}}(t), \quad (8)$$

where $\delta_{\mathrm{L}}(t)$ is the component of the baseline linear controller and $\delta_{\mathrm{ad}}(t)$ is the adaptive increment. Feedback/feedforward gains for the baseline (nominal) inner-loop controller are designed in Lavretsky and Wise (2005) assuming no modelling uncertainties, (i.e. $\Lambda = I_3$ and $K_0(x_p) = 0_{3\times 1}$) using the robust servomechanism LQR method with output projection (Wise 1990; Wise and Deylami 1991; Wise and Brinker 1996). The corresponding inner-loop control system takes the form:

$$\delta_{\mathrm{L}}(t) = K_x^\top x(t) + K_u^\top u(t), \quad (9)$$

where K_x and K_u denote the (9×3) and (4×3)– nominal feedback and feedforward gain matrices, correspondingly. Nominal inner-loop feedback when applied to the ideal model (1) (i.e. without uncertainties), leads to

$$A_m = A + B_1 K_x^\top, \quad B_m = B_2 + B_1 K_u^\top, \quad (10)$$

which characterise the desired transient and steady-state response for a given reference input $u(t)$:

$$\dot{x}_m(t) = A_m x_m(t) + B_m u(t). \quad (11)$$

We note that the choice of K_x and K_u has to render A_m Hurwitz and and provide unity DC gains from the commanded signals to the corresponding system outputs.

Using the stabilising gains for the inner-loop, the system in (1) takes the form:

$$\begin{aligned}\dot{x}(t) = &\left(A + B_1 \Lambda K_x^T\right) x(t) + B_1 \Lambda(\delta_{\mathrm{ad}} + K_0(x_p(t))) \\ &+ \left(B_2 + B_1 \Lambda K_u^T\right) u(t).\end{aligned} \quad (12)$$

From (10) and (12), we have

$$\begin{aligned}\dot{x}(t) = A_m x(t) + B_m u(t) + B_1 \Big(&\Lambda \delta_{\mathrm{ad}}(t) + \Lambda K_0(x_p(t)) \\ &+ k_x^\top x(t) + k_u^\top u(t) \Big),\end{aligned} \quad (13)$$

where

$$k_x^\top = (\Lambda - I) K_x^\top, \quad k_u^\top = (\Lambda - I) K_u^\top. \quad (14)$$

Remark 1: In the absence of actuator failures, i.e. when $\Lambda = I_3$, we have $k_x(t) = 0_{9\times 3}$ and $k_u(t) = 0_{4\times 3}$. This implies that the adaptive system augments the baseline inner-loop controller, and therefore the incremental adaptive feedback gains can be initialised at zero.

We note that, given a compact set $\mathcal{D}$, the non-linearity $\Lambda K_0(x_p)$ can be approximated using a feedforward NN:

$$\Lambda K_0(x_p) = w^\top \Phi(x_p) + \epsilon(x_p), \quad (15)$$

where $w \in \mathbb{R}^{\mathrm{N}_0 \times 3}$ is a matrix of unknown parameters that belongs to a known (conservative) compact set, $\Phi(x_p)$ is a vector of suitably chosen RBFs, $\|\epsilon(x_p)\|\epsilon_\infty \leq \epsilon^*$ is the uniformly bounded approximation error on $\mathcal{D}$. The set $\mathcal{D}$ will be introduced shortly. Next, we introduce the elements of the $\mathcal{L}_1$ neural adaptive controller.

State Predictor Model:

$$\begin{aligned}\dot{\hat{x}}(t) = A_m \hat{x}(t) + B_m u(t) + B_1 \Big(&\hat{\Lambda}(t) \delta_{\mathrm{ad}}(t) \\ &+ \hat{k}_x^\top(t) x(t) + \hat{w}^\top(t) \Phi(x_p(t)) + \hat{k}_u(t)^\top u(t) \Big).\end{aligned} \quad (16)$$

in which $\hat{\Lambda}(t)$, $\hat{k}_x(t)$, $\hat{w}(t)$, $\hat{k}_u(t)$ are the adaptive parameters.

Adaptive Laws:

$$\begin{aligned}\dot{\hat{\Lambda}}(t) &= \Gamma \mathrm{Proj}(\hat{\Lambda}(t), -\delta_{\mathrm{ad}}(t) \tilde{x}^\top(t) P B_1), \\ \dot{\hat{k}}_x(t) &= \Gamma \mathrm{Proj}(\hat{k}_x(t), -x(t) \tilde{x}^\top(t) P B_1), \\ \dot{\hat{w}}(t) &= \Gamma \mathrm{Proj}(\hat{w}(t), -\Phi(x_p(t)) \tilde{x}^\top(t) P B_1), \\ \dot{\hat{k}}_u(t) &= \Gamma \mathrm{Proj}(\hat{k}_u(t), -u(t) \tilde{x}^\top(t) P B_1),\end{aligned} \quad (17)$$

in which $\tilde{x}(t) = \hat{x}(t) - x(t)$ is the tracking error between the system dynamics in (1) and the state predictor in (16), Γ is positive adaptations gain, and $P = P^\top > 0$ is the solution of the algebraic Lyapunov equation

$A_m^\top P + P A_m = -Q$, $Q>0$, while Proj$(\cdot,\cdot)$ denotes the projection operator (Pomet and Praly 1992).

Control Law: The control signal is generated through gain feedback of the following system:

$$\chi(s) = D(s) r_u(s), \quad \delta_{\text{ad}}(s) = -k\chi(s), \tag{18}$$

where $r_u(s)$ is the Laplace transformation of $r_u(t) = \hat{\Lambda}(t)\delta_{\text{ad}}(t) + \bar{r}(t)$,

$$\bar{r}\Big(t = \hat{k}_x^\top(t)x(t) + \hat{k}_u^\top(t)u(t) + \hat{w}^\top(t)\Phi(x_p(t)\Big), \tag{19}$$

$k \in \mathbb{R}^{3\times 3}$ is positive diagonal feedback gain matrix

$$k = \begin{bmatrix} k_1 & 0 & 0 \\ 0 & k_2 & 0 \\ 0 & 0 & k_3 \end{bmatrix}, \tag{20}$$

and $D(s)$ is any diagonal transfer function

$$D(s) = \begin{bmatrix} D_1(s) & 0 & 0 \\ 0 & D_2(s) & 0 \\ 0 & 0 & D_3(s) \end{bmatrix} \tag{21}$$

that leads to strictly proper stable

$$C(s) = \begin{bmatrix} C_1(s) & 0 & 0 \\ 0 & C_2(s) & 0 \\ 0 & 0 & C_3(s) \end{bmatrix}, \qquad C_i(s) = \frac{\Lambda_i k_i D_i(s)}{1 + \Lambda_i k_i D(s)}, \quad i = 1,2,3 \tag{22}$$

with low-pass gain $C_i(0) = 1$. One simple choice is

$$D_i(s) = \frac{1}{s}, \tag{23}$$

which yields a first-order strictly proper $C(s)$ in the following form

$$C(s) = \begin{bmatrix} \dfrac{\Lambda_1 k_1}{s + \Lambda_1 k_1} & 0 & 0 \\ 0 & \dfrac{\Lambda_2 k_2}{s + \Lambda_2 k_2} & 0 \\ 0 & 0 & \dfrac{\Lambda_3 k_3}{s + \Lambda_3 k_3} \end{bmatrix}. \tag{24}$$

Further, let

$$L_x = \max\{|\Lambda_l - 1|, |\Lambda_u - 1|\}\|K_x^\top\|_{\mathcal{L}_1} = \max\{|\Lambda_l - 1|, |\Lambda_u - 1|\} \max_{i=1,2,3}\left(\sum_{j=1}^{9} |K_{x_{ji}}|\right), \tag{25}$$

$$L_u = \max\{|\Lambda_l - 1|, |\Lambda_u - 1|\}\|K_u^\top\|_{\mathcal{L}_1} = \max\{|\Lambda_l - 1|, |\Lambda_u - 1|\} \max_{i=1,2,3}\left(\sum_{j=1}^{9} |K_{u_{ji}}|\right),$$

where $K_{x_{ji}}(t)$ are the jth row ith column element of K_x. We now state the $\mathcal{L}_1$ performance requirement that ensures stability of the entire system and desired transient performance, as in Cao and Hovakimyan (2006c).

$\mathcal{L}_1$-gain requirement: Design $D(s)$ and k to satisfy

$$\|\bar{G}(s)\|_{\mathcal{L}_1} L < 1, \tag{26}$$

where

$$L = L_w + L_x, \tag{27}$$

$$\bar{G}(s) = (sI - A_m)^{-1} B_1 (I_{3\times 3} - C(s)), \tag{28}$$

in which L_w and L_x are defined in (5) and (25).

Since with RBF approximation the performance results are always local, one needs to characterise the set $\mathcal{D}$, on which the RBFs are distributed. Let

$$\mathcal{D} = \{x \mid \|x\|_\infty \le \gamma_r + \gamma_1 + \gamma_0 + \sigma\}, \tag{29}$$

where $\sigma > 0$ is an arbitrary positive constant, while

$$\gamma_r = \Big(\|H_m(s)\|_{\mathcal{L}_1}\|u\|_{\mathcal{L}_\infty} + \|\bar{G}(s)\|_{\mathcal{L}_1}\big(B + \epsilon^* + L_u\|u\|_{\mathcal{L}_\infty}\big) + \|H_o(s)\|_{\mathcal{L}_1}\epsilon^*\Big)\Big/\Big(1 - \|\bar{G}(s)\|_{\mathcal{L}_1} L\Big), \tag{30}$$

$$\gamma_0 = \sqrt{\frac{\lambda_{\max}(P)}{\lambda_{\min}(P)}\left(\frac{2\|PB_1\|}{\lambda_{\min}(Q)}\left(\epsilon^* + \frac{d_\Delta}{\Gamma}\right)\right)^2 + \frac{W_{\max}}{\lambda_{\min}(P)\Gamma}}, \qquad W_{\max} \triangleq \max_{W\in\Theta} 4\|W\|^2, \tag{31}$$

$$\gamma_1 = \frac{5\epsilon^*\|\bar{G}(s)\|_{\mathcal{L}_1} + \|H_o(s)\|_{\mathcal{L}_1}\epsilon^* + (1 + \|C(s) - 1\|_{\mathcal{L}_1})\gamma_0}{1 - \|\bar{G}(s)\|_{\mathcal{L}_1} L}, \tag{32}$$

where

$$H_m(s) \triangleq (sI - A_m)^{-1} B_m, \qquad H_o(s) \triangleq (sI - A_m)^{-1} B_1, \tag{33}$$

$$W^\top \triangleq \big[\Lambda \; k_x^\top \; w^\top \; k_u^\top\big], \tag{34}$$

and Θ is the compact set to which W belongs. The complete $\mathcal{L}_1$ neural adaptive controller consists of (8), (9), (16–18) subject to (26) with $\mathcal{D}$ defined in (29). The closed-loop system with it is illustrated in Figure 1.

4. Analysis of $\mathcal{L}_1$ adaptive controller

The analysis of the $\mathcal{L}_1$ adaptive controller is based on Cao and Hovakimyan (2006, 2007). The main

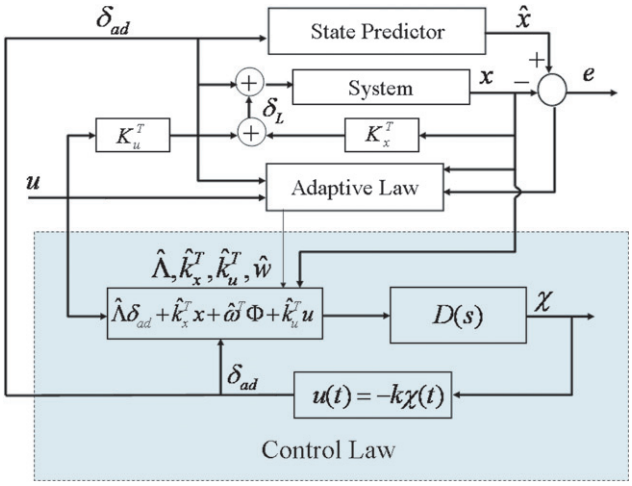

Figure 1. Closed-loop system with $\mathcal{L}_1$ neural adaptive controller.

difference as compared to Cao and Hovakimyan (2006c, 2007) is that the system in this article is multi-input and multi-output and has unknown high-frequency gain in each channel. As compared to Cao and Hovakimyan (2007) it has unknown non-linearities and uses RBFs for approximation.

4.1 *Closed-loop reference system*

We now consider the following closed-loop LTI reference system with its control signal and system response being defined as follows:

$$\dot{x}_{\text{ref}}(t) = A_m x_{\text{ref}}(t) + B_m u(t) + B_1\Big(\Lambda\delta_{\text{ad}_{\text{ref}}}(t) + k_x^\top x_{\text{ref}}(t) + w^\top \Phi(x_{p_{\text{ref}}}(t)) + \epsilon(x_{p_{\text{ref}}}(t)) + k_u^\top u(t)\Big) \tag{35}$$

$$\delta_{\text{ad}_{\text{ref}}}(s) = \Lambda^{-1}C(s)\eta_1(s), \quad x_{\text{ref}}(0) = x_0, \tag{36}$$

where $\eta_1(s)$ is the Laplace transformation of the signal

$$\eta_1(t) = -\big(k_x^\top x_{\text{ref}}(t) + w^\top(t)\Phi(x_{p_{\text{ref}}}(t)\big) + k_u^\top u(t)),$$

and $x_{p_{\text{ref}}}$ presents some of the components of the state x_{ref}, as it was for x_p and x. The control law in (36) leads to the following closed-loop dynamics:

$$\begin{aligned} x_{\text{ref}}(s) &= H_m(s)u(s) + \bar{G}(s)\eta_1(s) + H_o(s)\epsilon(s) \\ y_{\text{ref}}(s) &= c^\top x_{\text{ref}}(s), \end{aligned} \tag{37}$$

where $r(s)$, $\epsilon(s)$, and $\eta_1(s)$ are the Laplace transformation of signals $r(t)$, $\epsilon(x_{\text{ref}}(t))$ and $\eta_1(t)$, and $x_{\text{ref}}(0) = x_0$.

The next Lemma establishes stability of the closed-loop system in (35) and (36).

Lemma 1: *The control signal given by* (36), *subject to the condition in* (26) *ensures that the state of the closed-loop system in* (35) *remains inside* $\mathcal{D}$ *for all* $t \geq 0$, *i.e.*

$$\|x_{\text{ref}}\|_{\mathcal{L}_\infty} \leq \gamma_r, \tag{38}$$

where γ_r *is defined in* (30).

Proof: We will prove the lemma by contradiction. Assume that (38) is not true. Since $\|x_{\text{ref}}(0)\|_\infty = 0 \leq \gamma_r$ and $x_{\text{ref}}(t)$ is continuous, there exists t' such that $\|x_{\text{ref}}(t')\|_\infty > \gamma_r$ and $\|x_{\text{ref}}(\tau)\|_\infty \leq \gamma_r + \gamma_1$ for any $\tau \in [0, t']$, which consequently leads to the following inequalities for $\|x_{\text{ref}_{t'}}\|_{\mathcal{L}_\infty}$:

$$\gamma_r < \|x_{\text{ref}_{t'}}\|_{\mathcal{L}_\infty} \leq \gamma_r + \gamma_1. \tag{39}$$

It follows from (29) that

$$x_{\text{ref}}(\tau) \in \mathcal{D}, \quad \forall \tau \in [0,\ t'].$$

For the closed-loop system state in (37), we have

$$\|x_{\text{ref}_{t'}}\|_{\mathcal{L}_\infty} \leq \|H_m(s)\|_{\mathcal{L}_1}\|u_{t'}\|_{\mathcal{L}_\infty} + \|\bar{G}(s)\|_{\mathcal{L}_1}\|\eta_{1_{t'}}\|_{\mathcal{L}_\infty} + \|H_o(s)\|_{\mathcal{L}_1}\epsilon^*. \tag{40}$$

It follows from the definition of $\eta_1(\tau)$ that

$$\eta_1(\tau) = k_x^\top x_{\text{ref}}(t) + k_u^\top u(t) + f(x_{p_{\text{ref}}}(\tau)) - \epsilon(x_{p_{\text{ref}}}(\tau)),$$

for all $\tau \in [0, t']$ and, hence

$$\|\eta_{1_{t'}}\|_{\mathcal{L}_\infty} \leq |f(0)|_\infty + L\|x_{\text{ref}_{t'}}\|_{\mathcal{L}_\infty} + \epsilon^* + L_u\|u_{t'}\|_{\mathcal{L}_\infty}.$$

This consequently leads to the next upper bound for the expression in (40).

$$\|x_{\text{ref}_{t'}}\|_{\mathcal{L}_\infty} \leq \|H_m(s)\|_{\mathcal{L}_1}\|u_{t'}\|_{\mathcal{L}_\infty} + \|H_o(s)\|_{\mathcal{L}_1}\epsilon^* + \|\bar{G}(s)\|_{\mathcal{L}_1}\big(|f(0)|_\infty + L\|x_{\text{ref}_{t'}}\|_{\mathcal{L}_\infty} + \epsilon^* + L_u\|u_{t'}\|_{\mathcal{L}_\infty}\big). \tag{41}$$

Using the condition in (26) and the upper bound in (4), one gets:

$$\|x_{\text{ref}_{t'}}\|_{\mathcal{L}_\infty} \leq \Big(\|H_m(s)\|_{\mathcal{L}_1}\|u_{t'}\|_{\mathcal{L}_\infty} + \|\bar{G}(s)\|_{\mathcal{L}_1}\big(B + \epsilon^* + L_u\|u_{t'}\|_{\mathcal{L}_\infty}\big) + \|H_o(s)\|_{\mathcal{L}_1}\epsilon^*\Big)/\Big(1 - \|\bar{G}(s)\|_{\mathcal{L}_1}L\Big).$$

Since $\|u_{t'}\|_{\mathcal{L}_\infty} \leq \|u\|_{\mathcal{L}_\infty}$, then it is straightforward to see that

$$\|x_{\text{ref}_{t'}}\|_{\mathcal{L}_\infty} \leq \gamma_r,$$

which contradicts $\gamma_r < \|x_{\text{ref}_{t'}}\|_{\mathcal{L}_\infty}$ in (39). Hence, the relationship in (38) holds, and this completes the proof. □

4.2 *Guaranteed transient performance of $\mathcal{L}_1$ NN adaptive controller*

If $x(\tau) \in \mathcal{D}$ for all $\tau \in [0, t]$, the RBF approximation in (15) holds and the system dynamics in (13) over this time interval can be rewritten as:

$$\begin{aligned}\dot{x}(t) &= A_m x(t) + B_m u(t) + B_1 \\ &\quad \underbrace{\begin{pmatrix}\Lambda & k_x^\top & w^\top & k_u^\top\end{pmatrix}}_{W^\top} \underbrace{\begin{pmatrix}\delta_{\text{ad}}(t) \\ x(t) \\ \Phi(x_p(t)) \\ u(t)\end{pmatrix}}_{-\psi(x,u,\delta_{\text{ad}})} + B_1 \epsilon(x_p(t)), \\ &= A_m x(t) + B_m u(t) - B_1 W^\top \psi(x(t), u(t), \delta_{\text{ad}}(t)) \\ &\quad + B_1 \epsilon(x_p(t)), \quad \tilde{x}(0) = 0, \end{aligned} \tag{42}$$

where W is defined in (34). Similarly, letting

$$\hat{W}^\top(t) \triangleq \left[\hat{\Lambda}(t)\ \hat{k}_x^\top(t)\ \hat{w}^\top(t)\ \hat{k}_u^\top(t)\right], \tag{43}$$

the state estimator in (16) can be simplified as:

$$\dot{\hat{x}}(t) = A_m \hat{x}(t) + B_m u(t) - B_1 \hat{W}(t) \psi(x(t), u(t), \delta_{\text{ad}}(t)). \tag{44}$$

Defining

$$\begin{aligned} B_r &\triangleq \left[B_1 \bar{B}_1\right], \\ H_r(s) &\triangleq (sI - A_m)^{-1} B_r, \\ C_r(s) &\triangleq \begin{bmatrix}\Lambda^{-1} C(s) & 0 \\ 0 & \bar{C}(s)\end{bmatrix}, \end{aligned} \tag{45}$$

where $\bar{C}(s)$ is an arbitrary diagonal strict proper transfer function and the choice of $\bar{B}_1$ renders $B_r \in \mathbb{R}^{9\times 9}$ full rank.

Theorem 1: *Given the system in* (1), *the reference system in* (35), (36), *and the* $\mathcal{L}_1$ NN *adaptive controller defined via* (8), (9), (16), (17), *and* (18) *subject to* (26), *we have*:

$$\|x - \hat{x}\|_{\mathcal{L}_\infty} \leq \gamma_0, \tag{46}$$

$$\|x - x_{\text{ref}}\|_{\mathcal{L}_\infty} \leq \gamma_1, \tag{47}$$

$$\|\delta_{\text{ad}} - \delta_{\text{ad}_{\text{ref}}}\|_{\mathcal{L}_\infty} \leq \gamma_2, \tag{48}$$

where

$$\begin{aligned}\gamma_2 &= \|\Lambda^{-1} C(s)\|_{\mathcal{L}_1} L \gamma_1 + \|\Lambda^{-1} C_r(s) H_r^{-1}(s)\|_{\mathcal{L}_1} \\ &\quad \left(\gamma_0 + \left\|H_o(s)\right\|_{\mathcal{L}_1} \epsilon^*\right). \end{aligned} \tag{49}$$

Proof: The proof will be done by contradiction. Assume that (47) is not true. Then, since $\|x(0) - x_{\text{ref}}(0)\|_\infty = 0 \leq \gamma_1$, and both $x(t)$ and $x_{\text{ref}}(t)$ are continuous, there exists t' such that $\|x(t') - x_{\text{ref}}(t')\|_\infty > \gamma_1$ and $\|x(\tau) - x_{\text{ref}}(\tau)\|_\infty \leq \gamma_1 + \sigma$ for any $\tau \in [0, t']$. This leads to the following inequalities:

$$\gamma_1 < \|(x - x_{\text{ref}})_{t'}\|_{\mathcal{L}_\infty} \leq \gamma_1 + \sigma, \tag{50}$$

which consequently implies that

$$x(\tau) \in \mathcal{D}, \quad \forall \tau \in [0, t'].$$

Since $x(\tau) \in \mathcal{D}$, and the regressor in the state predictor in (44) operates over x, one can use the relationships in (15) and (42) to derive the following error dynamics:

$$\begin{aligned}\dot{\tilde{x}}(t) &= A_m \tilde{x}(t) + B_1 \big(\tilde{\Lambda}(t)\delta_{\text{ad}}(t) + \tilde{k}_x^\top(t) x(t) + \tilde{w}^\top(t)\Phi(x_p(t)) \\ &\quad + \tilde{k}_u^\top(t) u(t) + \epsilon(x_p(t))\big), \ \tilde{x}(0) = 0, \end{aligned} \tag{51}$$

where

$$\tilde{w}(t) \triangleq \hat{w}(t) - w, \quad \tilde{k}_x(t) \triangleq \hat{k}_x(t) - k_x, \tag{52}$$

$$\tilde{k}_u(t) \triangleq \hat{k}_u(t) - k_u, \quad \tilde{\Lambda}(t) \triangleq \hat{\Lambda}(t) - \Lambda.$$

Letting $\tilde{W}(t) = \hat{W}(t) - W$, the error dynamics can be written in the form

$$\dot{\tilde{x}}(t) = A_m \tilde{x}(t) - B_1 \tilde{W}^\top(t) \psi(x(t), u(t), \delta_{\text{ad}}(t)) + B_1 \epsilon(x_p(t)). \tag{53}$$

Consider the following candidate Lyapunov function:

$$V(\tilde{x}(t), \tilde{W}) = \tilde{x}^\top(t) P \tilde{x}(t) + \Gamma^{-1} \text{trace}\big(\tilde{W}^\top \tilde{W}\big), \tag{54}$$

where $P = P^\top > 0$ is the solution of the algebraic Lyapunov equation $A_m^\top P + P A_m = -Q$, $Q > 0$. The following is straightforward to derive:

$$\dot{V}(\tau) \leq -\tilde{x}^\top(\tau) Q \tilde{x}(\tau) + 2\tilde{x}^\top(\tau) P B_1 \epsilon(x_p(\tau)), \ \forall \tau \in [0, t'].$$

Therefore, $\dot{V}(\tau) \leq 0$ for any $\tau \in [0, t']$ if

$$\|\tilde{x}(\tau)\|_\infty \geq \frac{2\epsilon^* \|P B_1\|_{\mathcal{L}_1}}{\lambda_{\min}(Q)}.$$

The projection algorithm ensures that $\hat{\mathbf{W}}(\tau) \in \Theta$, $\forall \tau \in [0, t']$, and therefore

$$\max_{\tau \in [0,t']} \Gamma^{-1} \tilde{W}^\top(\tau) \tilde{W}(\tau) \leq \frac{W_{\max}}{\Gamma},$$

where $W_{\max}$ is defined in (31). Thus $\dot{V}(\tau) \leq 0$, $\tau \in [0, t']$, outside the compact set:

$$\left\{\|\tilde{x}\|_\infty \leq \frac{2\epsilon^* \|P B_1\|_{\mathcal{L}_1}}{\lambda_{\min}(Q)}\right\} \bigcap \left\{\|\tilde{W}\| \leq \sqrt{W_{\max}}\right\}. \tag{55}$$

This consequently implies that for any $\tau \in [0, t']$

$$\|\tilde{x}(\tau)\| \leq \gamma_0 ,$$

and hence

$$\|\tilde{x}_{t'}\|_{\mathcal{L}_\infty} \leq \gamma_0. \tag{56}$$

Moreover, using the upper bounds in (50) and (38) along with $\|\tilde{x}(\tau)\| \leq \gamma_0$, implies that

$$\hat{x}(\tau) \in \mathcal{D}, \quad \forall \tau \in [0, t'].$$

From (16) and (37), one can write

$$\begin{aligned} \hat{x}(s) - x_{\text{ref}}(s) &= \bar{G}(s)(\bar{r}(s) - \eta_1(s)) - H_o(s)\epsilon(s) \\ &= \bar{G}(s)(\eta_2(s) - \eta_3(s) + \eta_4(s)) - H_o(s)\epsilon(s), \end{aligned} \tag{57}$$

where $\eta_2(s)$, $\eta_3(s)$, $\eta_4(s)$ are the Laplace transforms of $\tilde{W}^\top(t)\psi(x(t), u(t), \delta_{\text{ad}}(t))$, $W^\top\big((\psi(\hat{x}(t), u(t), \delta_{\text{ad}}) - \psi(x(t)(t), \delta_{\text{ad}}(t))\big)$, $W^\top\big(\psi(\hat{x}(t), u(t), \delta_{\text{ad}}) - \psi(x_{\text{ref}}(t), u(t), \delta_{\text{ad}})\big)$, respectively. The relationship in (51) leads to

$$\tilde{x}(s) = H_o(s)(-\eta_2(s) - \epsilon(s)). \tag{58}$$

Recalling the definition of $\bar{G}(s)$ from (28), one can further write

$$\begin{aligned} \hat{x}(s) - x_{\text{ref}}(s) = \bar{G}(s)(&-\eta_3(s) + \eta_4(s) + \epsilon(s)) \\ &- (C(s) - 1)\tilde{x}(s) + H_o(s)\epsilon(s). \end{aligned} \tag{59}$$

Recalling the RBF approximation in (15), one gets the following upper bound

$$\begin{aligned} &\| - W^\top(\psi(\hat{x}(t), u(t), \delta_{\text{ad}}(t)) - \psi(x(t), u(t), \delta_{\text{ad}}(t))) \\ &\quad - ((f(\hat{x}(\tau)) - f(x(\tau)))\|_\infty \leq 2\epsilon^*, \quad \tau \in [0,\ t'], \end{aligned} \tag{60}$$

where $f(x(t)) = \Lambda\delta_{\text{ad}}(t) + \Lambda K_0(x_p(t)) + k_x^\top(t) + k_u^\top u(t)$. Hence the relationship in (5) implies that

$$\begin{aligned} \|\eta_{3_{t'}}\|_{\mathcal{L}_\infty} &= \|\big(W^\top(\psi(\hat{x}, u, \sigma_{\text{ad}}) - \psi(x, u, \sigma_{\text{ad}}))\big)_{t'}\|_{\mathcal{L}_\infty} \\ &\leq \|(f(\hat{x}) - f(x))_{t'}\|_{\mathcal{L}_\infty} + 2\epsilon^* \leq L\|\tilde{x}_{t'}\|_{\mathcal{L}_\infty} + 2\epsilon^*. \end{aligned} \tag{61}$$

Similarly, we have

$$\|\eta_{4_{t'}}\|_{\mathcal{L}_\infty} \leq L\|(\hat{x} - x_{\text{ref}})_{t'}\|_{\mathcal{L}_\infty} + 2\epsilon^*. \tag{62}$$

The following upper bound follows from (61) and (62):

$$\begin{aligned} \|(\hat{x} - x_{\text{ref}})_{t'}\|_{\mathcal{L}_\infty} \leq \|\bar{G}(s)\|_{\mathcal{L}_1}(&L\|(\hat{x} - x_{\text{ref}})_{t'}\|_{\mathcal{L}_\infty} \\ &+ L\|\tilde{x}_{t'}\|_{\mathcal{L}_\infty} + 5\epsilon^*) + \|C(s) \\ &- 1\|_{\mathcal{L}_1}\|\tilde{x}_{t'}\|_{\mathcal{L}_\infty} + \|H_o(s)\|_{\mathcal{L}_1}\epsilon^*, \end{aligned}$$

which along with the condition in (26) reduces to

$$\begin{aligned} \|(\hat{x} - x_{\text{ref}})_{t'}\|_{\mathcal{L}_\infty} \leq \Big(&\|\bar{G}(s)\|_{\mathcal{L}_1}\big(L\|\tilde{x}_{t'}\|_{\mathcal{L}_\infty} + 5\epsilon^*\big) \\ &+ \|C(s) - 1\|_{\mathcal{L}_1}\|\tilde{x}_{t'}\|_{\mathcal{L}_\infty} \\ &+ \|H_o(s)\|_{\mathcal{L}_1}\epsilon^*\Big)/(1 - \|\bar{G}(s)\|_{\mathcal{L}_1}L). \end{aligned}$$

Since

$$\|(x - x_{\text{ref}})_{t'}\|_{\mathcal{L}_\infty} \leq \|(\hat{x} - x_{\text{ref}})_{t'}\|_{\mathcal{L}_\infty} + \|\tilde{x}_{t'}\|_{\mathcal{L}_\infty},$$

it follows from (56) that

$$\|(x - x_{\text{ref}})_{t'}\|_{\mathcal{L}_\infty} \leq \gamma_1 ,$$

which contradicts the condition in (50). Hence, the relationship in (47) holds. The upper bound in (46) follows from (47) and (56) directly.

To prove the bound in (48), we notice that from (36) and (18) one can derive

$$\delta_{\text{ad}}(s) - \delta_{\text{ad}_{\text{ref}}}(s) = -\Lambda^{-1}C(s)\eta_5(s) - \eta_6(s), \tag{63}$$

where

$$\eta_6(s) = \Lambda^{-1}C(s)\eta_2(s), \tag{64}$$

and $\eta_5(s)$ is the Laplace transformation of $k_x^\top x(t) + w^\top\psi(x(t)) - k_x^\top x_{\text{ref}}(t) - w^\top\psi(x_{\text{ref}})(t)$. Therefore, we have

$$\|\delta_{\text{ad}} - \delta_{\text{ad}_{\text{ref}}}\|_{\mathcal{L}_\infty} \leq \|\Lambda^{-1}C(s)\|_{\mathcal{L}_1}L\|x - x_{\text{ref}}\|_{\mathcal{L}_\infty} + \|\eta_6\|_{\mathcal{L}_\infty}. \tag{65}$$

Let

$$\eta_r(s) \triangleq \begin{bmatrix} \eta_6^\top(t) & 0_{1\times 6} \end{bmatrix}^\top, \tag{66}$$

$$\tilde{r}(t) \triangleq \begin{bmatrix} \eta_2^\top(t) & 0_{1\times 6} \end{bmatrix}^\top. \tag{67}$$

From (64) we have

$$\eta_r(s) = \Lambda^{-1}C_r(s)\tilde{r}(s), \tag{68}$$

while the definitions in (66) and (67) lead to

$$\|\eta_r\|_{\mathcal{L}_\infty} = \|\eta_6\|_{\mathcal{L}_\infty} , \tag{69}$$

$$\|\tilde{r}\|_{\mathcal{L}_\infty} = \|\eta_2\|_{\mathcal{L}_\infty}. \tag{70}$$

It follows from (45), (67) and (58) that

$$\tilde{x}(s) = -H_r(s)\tilde{r}(s) + H_o(s)\,\epsilon\,(s). \tag{71}$$

The relationship in (68) implies that

$$\eta_r(s) = \Lambda^{-1}C_r(s)H_r^{-1}(s)H_r(s)\,\tilde{r}\,(s), \tag{72}$$

which along with (71) leads to

$$\eta_r(s) = C_r(s)H_r^{-1}(s)(-\tilde{x}(s) + H_o(s)\,\epsilon\,(s)). \tag{73}$$

The non-singularity of the matrix B_r implies that

$$C_r(s)H_r^{-1}(s) = C_r(s)B_r(sI - A_m). \tag{74}$$

Since $C_r(s)$ is a diagonal matrix with all the elements strictly proper, it can be verified easily that $C_r(s)B_r(sI - A_m)$ is proper and hence the $\mathcal{L}_1$ gain

$$\|\Lambda^{-1}C_r(s)H_r^{-1}(s)\|_{\mathcal{L}_1} \tag{75}$$

is finite. Therefore, it follows from (71) that

$$\|\eta_r\|_{\mathcal{L}_\infty} \leq \left\|\Lambda^{-1}C_r(s)H_r^{-1}(s)\right\|_{\mathcal{L}_1}\left(\|\tilde{x}\|_{\mathcal{L}_\infty} + \left\|H_o(s)\right\|_{\mathcal{L}_1}\epsilon^*\right). \tag{76}$$

It follows from (46), (69) and (76) that:

$$\begin{aligned}\|\eta_6\|_{\mathcal{L}_\infty} &= \|\eta_r\|_{\mathcal{L}_\infty} \\ &\leq \left\|\Lambda^{-1}C_r(s)H_r^{-1}(s)\right\|_{\mathcal{L}_1}\left(\gamma_0 + \left\|H_o(s)\right\|_{\mathcal{L}_1}\epsilon^*\right),\end{aligned} \tag{77}$$

which, when substituted into (65), leads to (48). □

Remark 2: From the relationships in (38) and (47) it is straightforward to verify that

$$\|x\|_{L_\infty} \leq \gamma_r + \gamma_1\,,$$

and hence x(t) belongs to $\mathcal{D}$ for any $t \geq 0$.

Corollary 1: *Given the system in* (1) *and the* $\mathcal{L}_1$ *NN adaptive controller defined via* (8), (9), (16), (17), *and* (18) *subject to* (26), *we have*:

$$\lim_{\Gamma\to\infty,\epsilon^*\to 0}(x(t) - \hat{x}(t)) = 0\,, \quad \forall t \geq 0,$$

$$\lim_{\Gamma\to\infty,\epsilon^*\to 0}(x(t) - x_{\text{ref}}(t)) = 0\,, \quad \forall t \geq 0,$$

$$\lim_{\Gamma\to\infty,\epsilon^*\to 0}\left(\delta_{\text{ad}}(t) - \delta_{\text{ad}_{\text{ref}}}(t)\right) = 0\,, \quad \forall t \geq 0.$$

Hence, if the the approximation error of the RBF network is small enough, we can arbitrarily minimise the bounds between the signals of the closed-loop $\mathcal{L}_1$ adaptive system and the closed-loop reference system. Thus, the problem is reduced to design of $C(s)$ to ensure that the closed-loop reference system approximates the response in (11). We note that the control law $\delta_{\text{ad}_{\text{ref}}}(t)$ in the closed-loop reference system, which is used in the analysis of $\mathcal{L}_\infty$ norm bounds, is not implementable since its definition involves the unknown parameters. Theorem 1 ensures that the $\mathcal{L}_1$ adaptive controller approximates $\delta_{\text{ad}_{\text{ref}}}(t)$ both in transient and steady state. So, it is important to understand how these bounds can be used for ensuring uniform transient response with *desired* specifications. We notice that the following *ideal* control signal $\delta_{\text{ideal}}(t) = \Lambda^{-1}\eta_1(t)$ is the one that cancels the uncertainties exactly leading to (11), provided the NN approximation is accurate enough. In the closed-loop reference system (35), $\delta_{\text{ideal}}(t)$ is further low-pass filtered by $C(s)$ to have guaranteed low-frequency range. In Cao and Hovakimyan (2006b) specific design guidelines are provided for selection of $C(s)$ to ensure that the reference system in (35) tracks the response of the desired system in (11). One way to achieve this is via the selection of a strictly proper system $C(s)$ that minimises the $\mathcal{L}_1$-gain of the cascaded system $C(s)(1 - C(s))$. We also notice that for any finite L, the condition in (26) can always be satisfied by increasing the bandwidth of $C(s)$. However, as proven in Cao and Hovakimyan (2007b) large bandwidth of $C(s)$ will hurt the time-delay margin.

Remark 3: Notice that if we set $C(s) = I_{3\times 3}$, then the $\mathcal{L}_1$ neural controller reduces to the MRAC type. In that case $\|\Lambda^{-1}H_r^{-1}(s)\|_{\mathcal{L}_1}$ cannot be finite since $H_r(s)$ is strictly proper. Therefore, from (49) it follows that $\gamma_2 \to \infty$, and hence for the control signal in conventional MRAC-type NN adaptive controller, one cannot reduce the bound in (48) by increasing the adaptive gain.

Remark 4: Recall that in conventional MRAC scheme the ultimate bound is given by γ_0 defined in (31). Notice that γ_0 depends upon ϵ^*, $W_{\max}$ and Γ. While ϵ^* and $W_{\max}$ are interconnected via the choice of RBFs, Γ is a design parameter of the adaptive process that can be used to reduce the ultimate bound. However, increasing Γ in the conventional MRAC scheme leads the control signal into high-frequency oscillations. With the $\mathcal{L}_1$ adaptive control architecture, the ultimate bound of the tracking error is given by γ_1 in (47). From the definition of it in (32), it follows that $\gamma_1 > \gamma_0$. Nevertheless, the ability of the $\mathcal{L}_1$ control architecture to tolerate large adaptive gain implies that γ_0 can be reduced leading to overall a smaller value for γ_1. This is enabled via the low-pass system $C(s)$ in the feedback path that filters out the high-frequencies in $\bar{r}(t)$ excited by large Γ. The $\mathcal{L}_1$ adaptive control architecture gives a scheme for fast adaptation without generating high-frequency oscillations in the control signal.

5. Simulation results

This section compares the performance of the nominal plant in the presence of pitch break and actuator failure with two adaptive control schemes: MRAC, which corresponds to $C(s) = 1$ defined in (22) and $\mathcal{L}_1$ adaptive controller. For MRAC, we reproduce the results of Lavretsky and Wise (2005). For the $\mathcal{L}_1$ adaptive controller, we set $k_i = 20$, for $i = 1$, 2, 3 and

$D(s) = (1/s)$, which verifies the $\mathcal{L}_1$ gain stability condition, and we set $\Gamma = 50{,}000$. Note that this leads to the same $C(s)$, as reported in Patel et al. (2007).

The performance of the $\mathcal{L}_1$ controller is compared to the performance of the baseline inner-loop controller and to the performance of MRAC. The results are shown in Figures 2–4. For comparison purposes, simulation data are obtained from the following three closed-inner-loop systems: (a) adaptation OFF, failures OFF (blue), (b) adaptation OFF, failures ON (red), (c) MRAC adaptation ON, failures ON (black) and (d) $\mathcal{L}_1$ adaptation ON, failures ON (Magenta).

Figures 2–4 demonstrate the benefits of adaptation, when the right outboard (ROB) elevon fails at 1 s of the maneoeuvre, and the pitch break phenomenon is active throughout the entire maneoeuvre. Figure 2 indicates that in spite of the unknown control failure and pitch break uncertainty, both MRAC and $\mathcal{L}_1$ adaptive systems are able to quickly reconfigure and track the commanded vertical acceleration, sideslip angle, roll rate and yaw rate signals, simultaneously. In fact, Figure 2 shows that with the adaptation turned on the desired/nominal system tracking behaviour has been almost recovered. In addition, Figure 3 compares the three virtual control feedback signals, and Figure 4 confirms that the level of control activity is reasonable, and that no control saturation has occurred during the adaptation process. In Figure 5, the subplot of Figure 2 is re-plotted to show the perfect tracking achieved by $\mathcal{L}_1$ as compared to MRAC for vertical acceleration.

Figures 6–8 demonstrate the benefits of adaptation when the inner-loop system receives repetitive vertical acceleration commands in the presence of both the ROB elevon failure and the unknown pitch break phenomenon. In Lavretsky and Wise (2005) it has been argued that the MRAC adaptive process quickly dampens the oscillations caused by the uncertainties and significantly reduces the corresponding control activity if repetitive commands are given to the system. However, from the zoomed Figure 9 it can be seen that the repetitive command is not necessary for the $\mathcal{L}_1$ architecture, since it has guaranteed transient performance from the beginning. In Figure 9, MRAC response is also plotted. For MRAC, we can see that there is small reduction in overshoot in vertical acceleration in the second pulse (20 s time instance) as compared to the first pulse command signal (1 s time instance).

Next we discuss robustness of two schemes. The time-delay margin for the inner loop (i.e. without adaptive feedback) can be computed from the phase margin of the open-loop transfer functions.

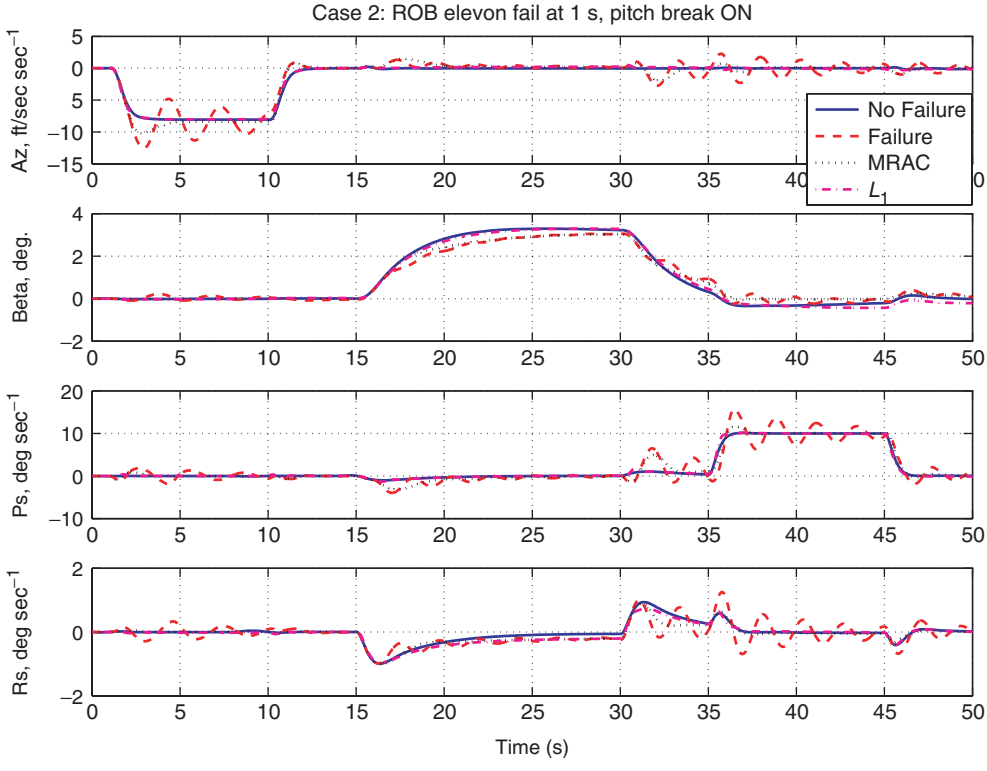

Figure 2. Inner-loop adaptation with ROB elevon failure and pitch break phenomenon: command tracking.

The open-loop transfer functions are calculated by breaking the virtual control $(\dot{p}, \dot{q}, \dot{r})$ command loops one at a time keeping the other two loops closed. This is shown in Table 1.

To calculate the time-delay margin for the adaptive systems, we introduce the time-delay at the plant input, and compute the margins using numerical simulations. The time-delay margins for MRAC are summarised

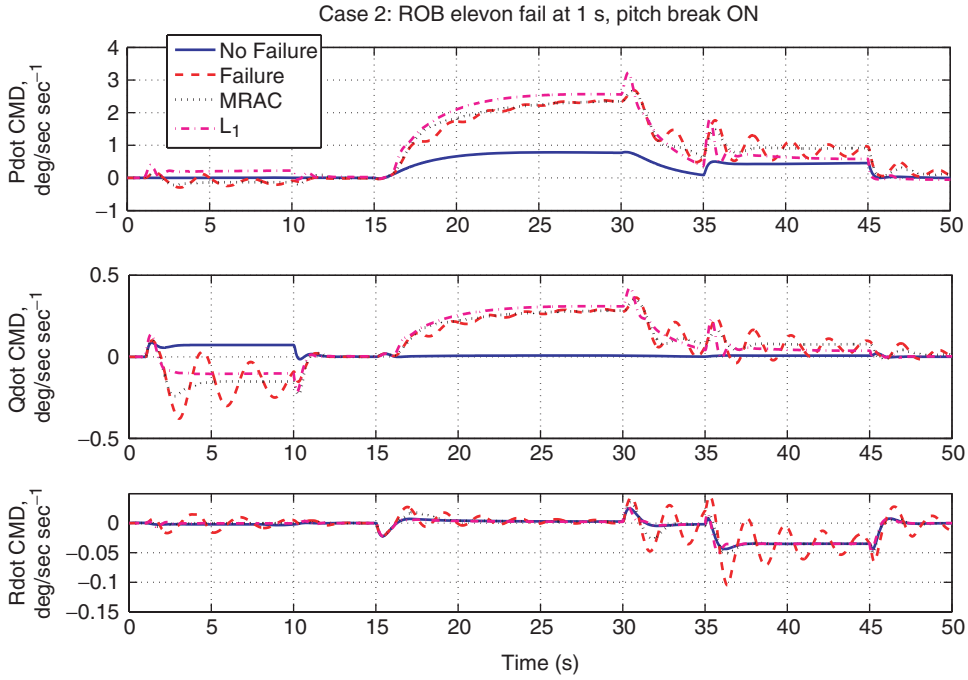

Figure 3. Inner-loop adaptation with ROB elevon failure and pitch break phenomenon: virtual controls.

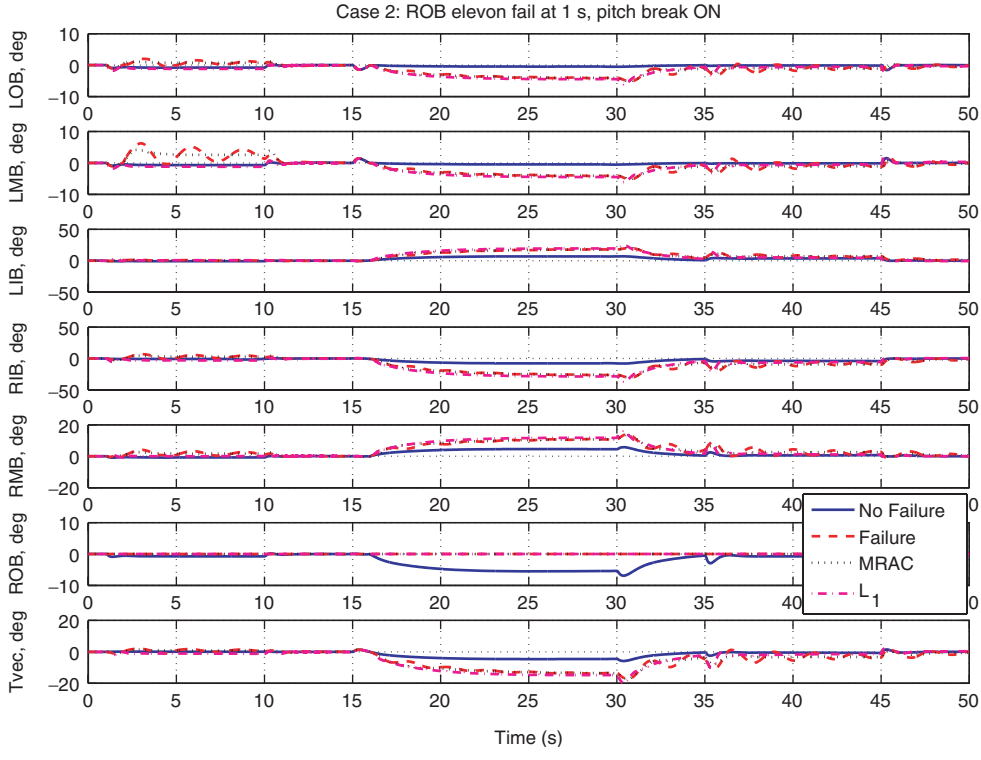

Figure 4. Inner-loop adaptation with ROB elevon failure and pitch break phenomenon: controls.

in Table 2. We can see that the worst case time-delay margin is 0.12 s (the adaptation parameter used in Lavretsky and Wise (2005) for MRAC scheme is 100).

The time-delay margins for $\mathcal{L}_1$ adaptive scheme are summarised in Table 3 for $C(s) = 1/(0.05s + 1)$ and $\Gamma = 50{,}000$. The worst case time-delay margin is 0.0425 s, which is smaller than the worst margin of MRAC scheme. Now, we discuss how to improve the time-delay margin by the change of $C(s)$ using the analysis from Cao and Hovakimyan (2007b).

Figure 5. Zoomed subplot of Figure 2 to show guaranteed $\mathcal{L}_1$ performance.

The time-delay margin for the $\mathcal{L}_1$ adaptive scheme for systems linearly dependent upon unknown parameters (i.e. in the absence of non-linearities and RBFs), can be computed analytically as $\Gamma \to \infty$ (Cao and Hovakimyan 2007b). In Cao and Hovakimyan (2007b) $C(s)/(1 - C(s))$ appears as a multiplier in the open-loop transfer function used for calculation of the time-delay margin for the $\mathcal{L}_1$ adaptive scheme. It is obvious that one could choose $C(s)$ judiciously to maximise the phase margin of the open-loop transfer function and minimise the cross-over frequency to obtain larger time-delay margin. Towards that end, consider the following low-pass filter

$$C_1(s) = \frac{1}{0.05s + 1} \frac{(-6s + 1)^2}{(8s + 1)^2},$$

for which the $\mathcal{L}_1$ gain requirement holds. The corresponding $D_1(i)$ will be

$$D_1(s) = \frac{(-6s + 1)^2}{s(3.2s^2 + 28.8s + 28.05)}.$$

The Bode plots of $D(s)$ and $D_1(s)$ are given in Figure 10. Note that a non-minimum phase filter is used to enhance the phase characteristic in the region of frequency-band in order to improve the phase margin.

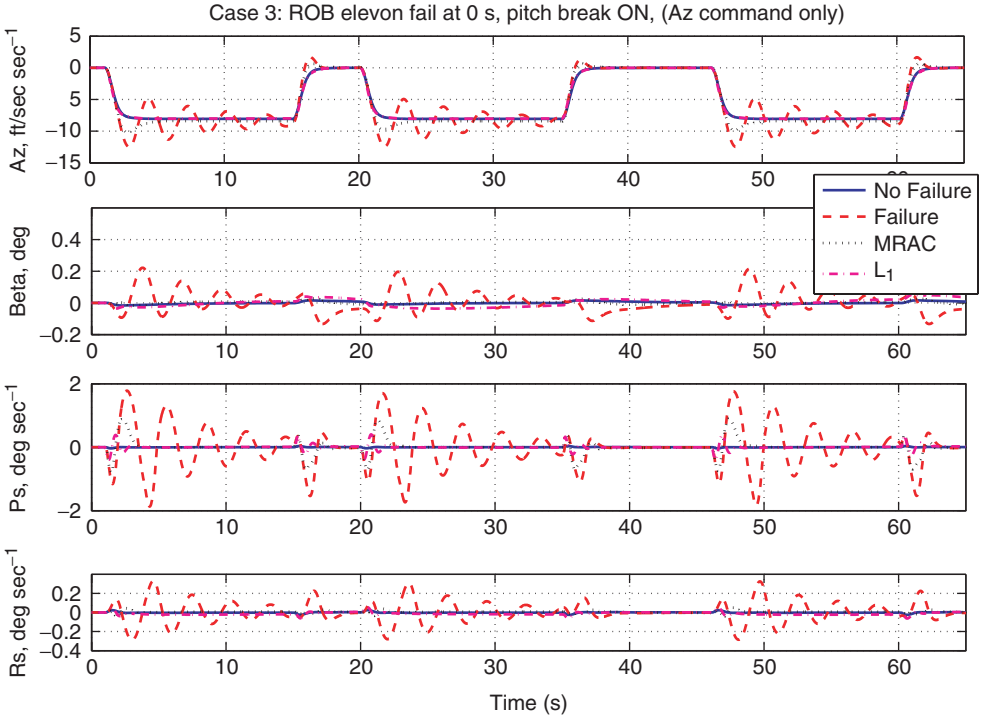

Figure 6. Inner-loop adaptation with vertical acceleration commands, ROB elevon failure, and pitch break phenomenon: command tracking.

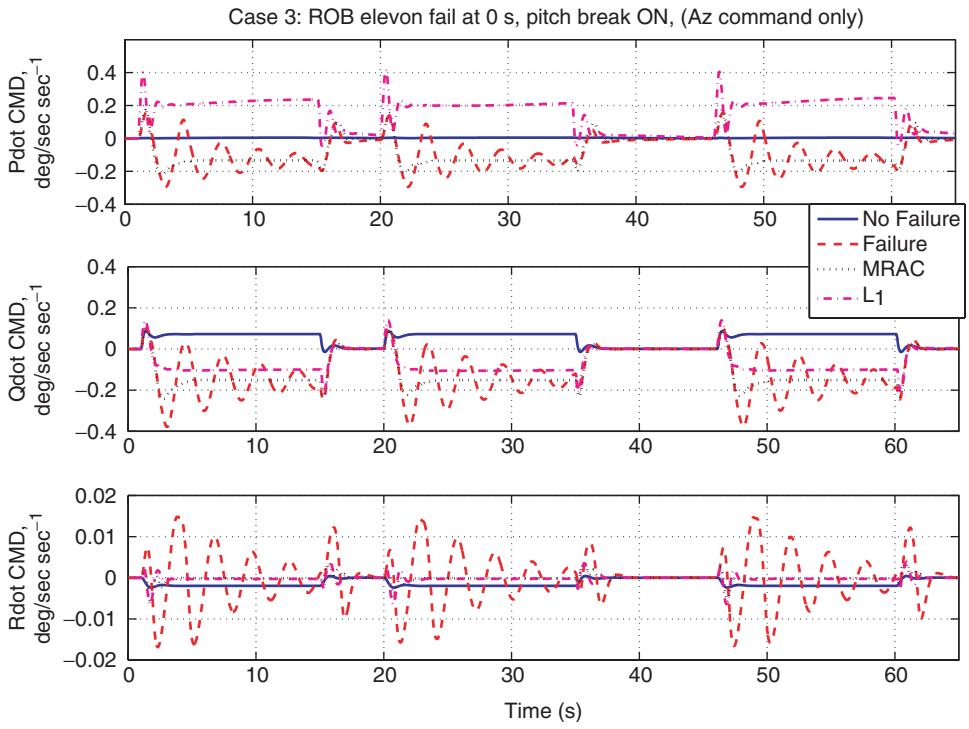

Figure 7. Inner-loop adaptation with vertical acceleration commands, ROB elevon failure and pitch break phenomenon: virtual controls.

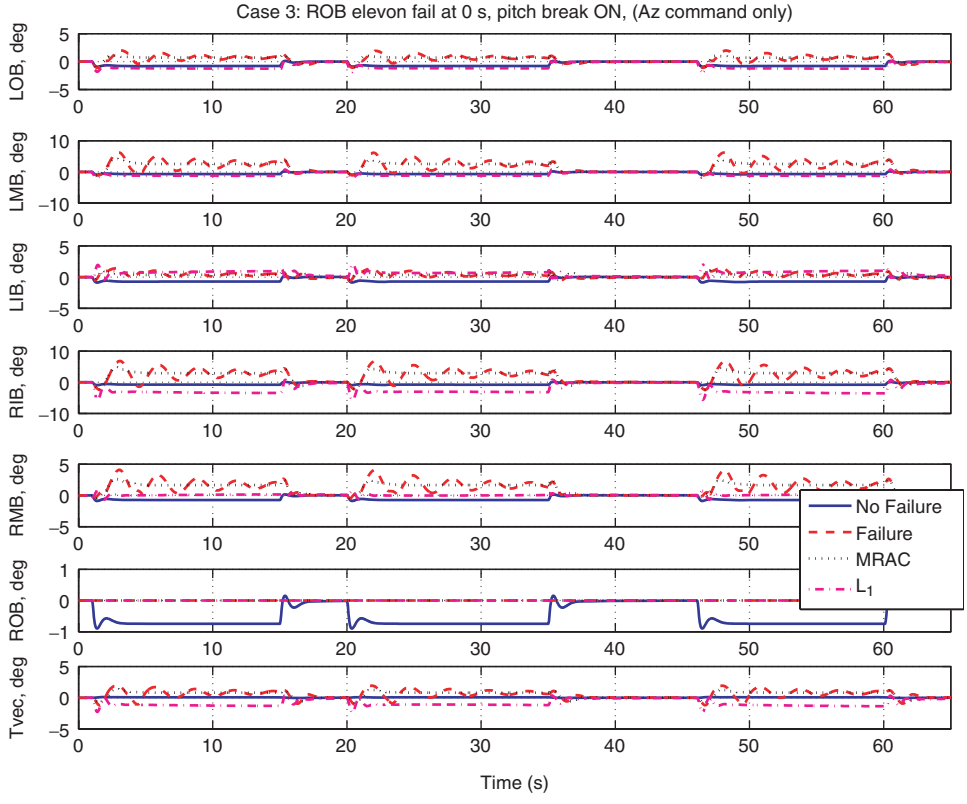

Figure 8. Inner-loop adaptation with vertical acceleration commands, ROB elevon failure and pitch break phenomenon: controls.

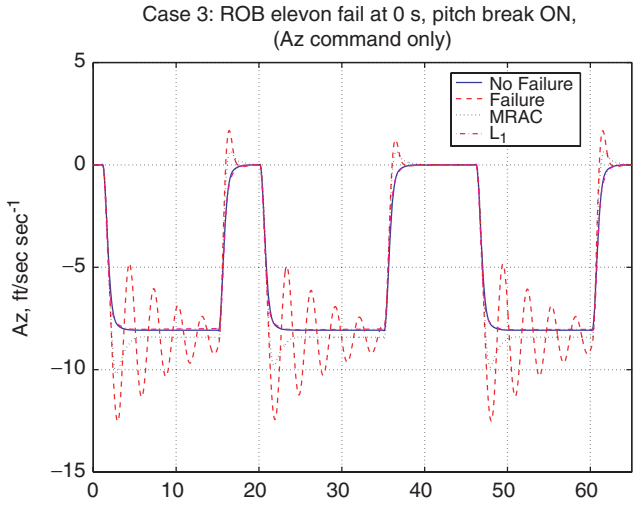

Figure 9. $\mathcal{L}_1$ does not need repetitive commands to learn.

Table 1. Phase and time-delay margins for the inner loop.

Loop margin	$\dot{p}$	$\dot{q}$	$\dot{r}$
Phase margin (deg.)	85.6	65.6	66.1
Cross-over frequency (rad s^{-1})	4.25	6.01	4.27
Time-delay margin (s)	0.3515	0.1905	0.2702

The subplot of vertical acceleration of Figure 2 is repeated with $C_1(s)$ in Figure 11. We see that there is some degradation in the tracking; however it is still better than MRAC. For this choice of $C_1(s)$, the worst case time-delay obtained from simulation is 0.10 s. In Table 2, we have the worst case time-delay margin for $C(s)$ equal to 0.0425 s, which implies that $C_1(s)$ doubles the time-delay margin. Thus, at this stage, it appears that improving the time-delay margin hurts the transient performance. The worst case time-delay margin for MRAC is 0.12, which is comparable to the worst-case margin of $C_1(s)$ in the presence of large adaptive gain $\Gamma = 50{,}000$. We note that all the time-delay margins are calculated for the ROB actuator failure case and in the presence of the pitch break uncertainty.

However, we note that a smaller value of Γ is preferable from an implementation point of view. Figure 12 shows the system response for different values of Γ for both low-pass filters. It can be seen that there is almost no degradation in the time-response performance. However, for the low-pass filter $C(s) = 1/(0.05s + 1)$, if we decrease Γ from 50,000 to 5000, the worst case time-delay margin decreases from 0.0425 to 0.003 (i.e. almost 14 times, much poorer than MRAC). However, for $C_1(s)$ it decreases from 0.10 to 0.07 (i.e only 1.4 times). Thus, with smaller choice of Γ, $C_1(s)$ is much suitable in terms of robustness as compared to $C(s)$. Table 4 summarises the margins for $C_1(s)$ with $\Gamma = 5000$.

Finally, we simulate the system with two actuator failures without any delays to test robustness of the two adaptive control schemes towards a different class of uncertainty. Figure 13 plots the vertical acceleration command tracking in the presence of pitch break uncertainty and ROB and LMB elevon

Table 2. Time-delay margin for MRAC.

$\dot{p}$	$\dot{q}$	$\dot{r}$	
0	0.18	0	Individual
0.33	0	0	Individual
0	0	0.20	Individual
0.16	0.16	0	Two loops
0	0.13	0.13	Two loops
0.17	0	0.17	Two loops
0.12	0.12	0.12	Simultaneous

Table 3. Time-delay margin for $\mathcal{L}_1$ for $C(s) = 1/(0.05s + 1)$.

$\dot{p}$	$\dot{q}$	$\dot{r}$	
0	0.055	0	Individual
0.0691	0	0	Individual
0	0	0.05645	Individual
0.0432	0.0432	0	Two loops
0	0.0455	0.0455	Two loops
0.05325	0	0.05325	Two loops
0.0425	0.0425	0.0425	Simultaneous

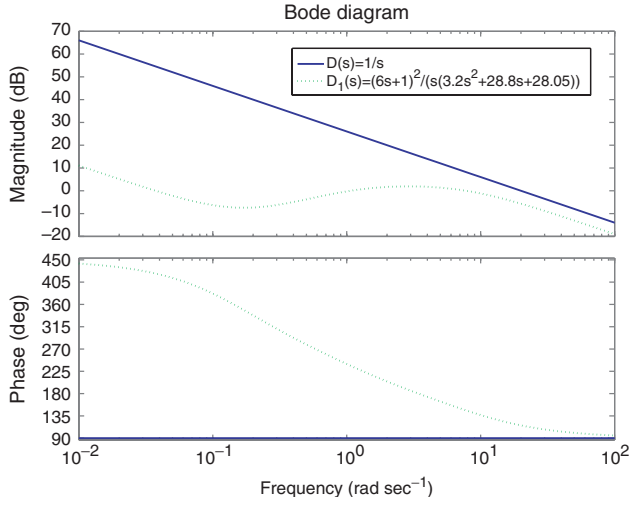

Figure 10. Choice of $C(s)$ to maximise the time-delay margin.

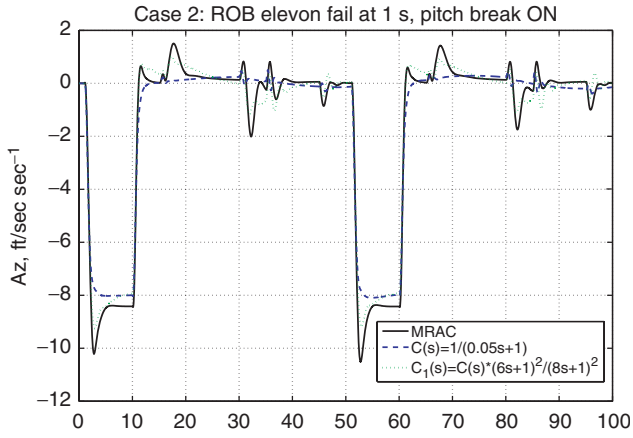

Figure 11. Inner-loop adaptation with ROB elevon failure and pitch break phenomenon: command tracking (for different choice of $C(s)$).

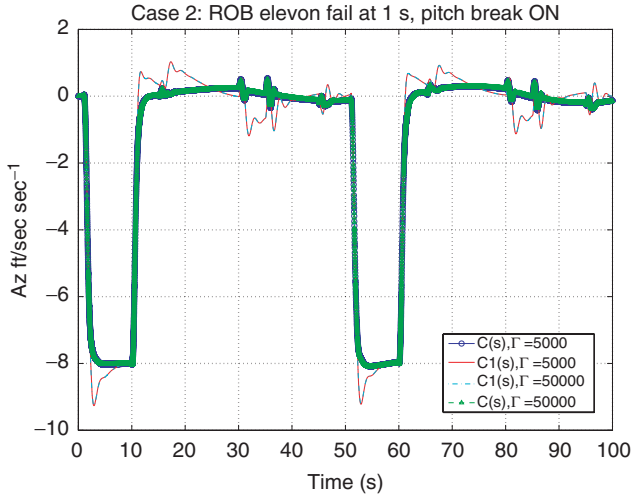

Figure 12. Inner-loop adaptation with ROB elevon failure and pitch break phenomenon: command tracking (for different values of Γ).

Table 4. Time-delay margin of $\mathcal{L}_1$ for $C_1(s)$ and $\Gamma = 5000$.

$\dot{p}$	$\dot{q}$	$\dot{r}$	
0	0.14	0	Individual
0.2	0	0	Individual
0	0	0.19	Individual
0.09	0.09	0	Two loops
0	0.09	0.09	Two loops
0.12	0	0.12	Two loops
0.07	0.07	0.07	Simultaneous

failures. We see that despite of the reasonably good time-delay margins in Table 2, MRAC loses stability, while the $\mathcal{L}_1$ adaptive control architecture retains both its tracking property and as well the worst

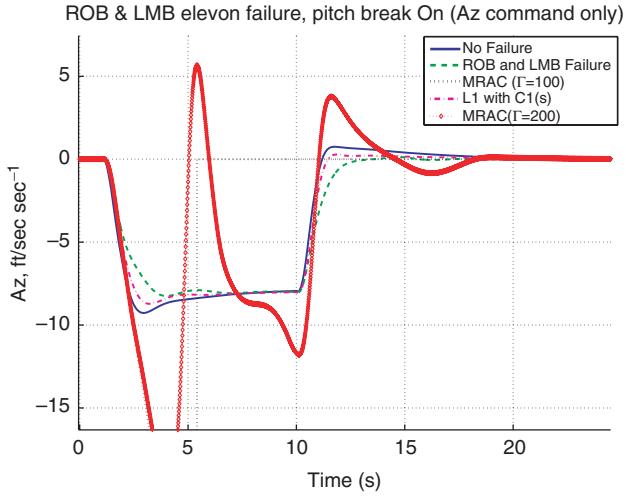

Figure 13. MRAC loses stability in the presence of two actuator failures, while $\mathcal{L}_1$ proves guaranteed tracking.

Table 5. Worst-case time-delay margin with single and double actuator failures.

Single	Double		Γ
0.11	<0.01	MRAC	200
0.12	Unstable	MRAC	100
0.0425	0.0425	$C(s)$	50,000
0.0225	0.0225	$C(s)$	5000
0.1	0.1233	$C_1(s)$	50,000
0.07	0.085	$C_1(s)$	5000

time-delay margin of 0.07, as predicted by the $\mathcal{L}_1$ theory. We further set $\Gamma = 200$ in MRAC to recover its performance, however, the performance is very poor. In Table 5, we have summarised the worst-case time-delay margins for single actuator and two actuator failures.

6. Conclusion

This article presents application of a novel $\mathcal{L}_1$ adaptive control architecture to an unstable tailless military aircraft. The robustness properties of the new architecture are compared with the conventional MRAC architecture, which shows that the $\mathcal{L}_1$ adaptive controller can be designed to improve the transient command tracking and increase the robustness to time-delay.

Acknowledgements

This material is based upon work supported by the United States Air Force under Contracts No. FA8650-05-C-3563,

FA9550-05-1-0157, FA9550-04-C-0047 and ONR under Contract N00014-05-1-0828. Any opinions, findings and conclusions or recommendations expressed in this material are those of the authors and do not necessarily reflect the views of the United States Air Force and ONR.

References

Brinker, J., and Wise, K.A. (2000), 'Flight Testing of a Reconfigurable Flight Control Law on the X-36 Tailless Fighter Aircraft', in *Proceedings of the AIAA GNC Conference*, Denver, CO.

Cao, C., and Hovakimyan, N. (2006a), 'Design and Analysis of a Novel $\mathcal{L}_1$ Adaptive Control Architecture, Part I: Control Signal and Asymptotic Stability', in *Proceedings of American Control Conference*, Minneapolis, MN, pp. 3397–3402.

Cao, C., and Hovakimyan, N. (2006b), 'Design and Analysis of a Novel $\mathcal{L}_1$ Adaptive Control Architecture, Part II: Guaranteed Transient Performance', in *Proceedings of American Control Conference*, Minneapolis, MN, pp. 3403–3408.

Cao, C., and Hovakimyan, N. (2006c), 'Novel $\mathcal{L}_1$ Neural Network Adaptive Control Architecture with Guaranteed Transient Performance', *IEEE Transactions on Neural Networks* 18, 1160–1171.

Cao, C., and Hovakimyan, N. (2007a), 'Guaranteed Transient Performance with $\mathcal{L}_1$ Adaptive Controller for Systems with Unknown Time-varying Parameters and Bounded Disturbances', *American Control Conference*, New York City, NY, pp. 3925–3930.

Cao, C., and Hovakimyan, N. (2007b), 'Stability Margins of $\mathcal{L}_1$ Adaptive Control Architecture', in *American Control Conference*, New York City, NY, pp. 3931–3936.

Cao, C., Patel, V.V., Reddy, C.K., Hovakimyan, N., Lavretsky, E., and Wise., K. (2006), 'Are Phase and Time-delay Margins Always Adversely Affected by High-Gain?', *AIAA Guidance, Navigation, and Control Conference*, AIAA Paper No. 2006-6347.

Corban, J., Burkemper, V., Holt, K., Evers, J., Calise, A., and Sharma, M. (2002), 'Flight Test of an Adaptive Autopilot for Precision Guided Munitions', *Proceedings of the AIAA Missile Sciences Conference*, Monterey, CA, pp. 5–7.

Kim, B.S., and Calise, A.J. (1997), 'Nonlinear Flight Control Using Neural Networks', *Journal of Guidance, Control and Dynamics*, 52, 26–33.

Lavretsky, E., and Hovakimyan, N. (2004), 'Positive-Modification for Stable Adaptation in a Class of Nonlinear Systems with Actuator Constraints', *Proceedings of American Control Conference*, Boston, MA, pp. 2545–2550.

Lavretsky, E., and Wise, K. (2005), 'Adaptive Flight Control for Manned/Unmanned Military Aircraft', *Proceedings of American Control Conference*, Portland, OR.

McFarland, M., and Calise, A. (1996), 'Neural-adaptive Nonlinear Autopilot Design for an Agile Anti-air Missile', in *Proceedings of the AIAA GNC Conference*, San Diego, CA, Paper AIAA 96-3914.

McFarland, M., and Calise, A. (1997), 'Multi-layer Neural Networks and Adaptive Non-linear Control of for Agile Anti-air Missiles', *Proceedings of the AIAA GNC Conference*, New Orleans, LA, Paper AIAA 97-3540.

Patel, V., Cao, C., Hovakimyan, N., Wise, K., and Lavretsky, E. (2007), '$\mathcal{L}_1$ Adaptive Controller for Tailless Unstable Aircraft', *American Control Conference*, New York City, NY, pp. 5272–5277.

Pomet, J.B., and Praly, L. (1992), 'Adaptive Nonlinear Regulation: Estimation from Lyapunov Equation', *IEEE Transctions on Automatic Control*, 37, 729–740.

Sharma, M., and Calise, A. (2001), 'Neural Network Augmentation of Existing Linear Controllers', *Proceedings of the AIAA GNC Conference*, Montreal, Canada, AIAA Paper No, 2001-4163.

Sharma, M., Calise, A.J., and Corban, J.E. (2000), 'Application of an Adaptive Autopilot Design to a Family of Guided Munitions', in *Proceedings of the AIAA GNC Conference*, Denver, CO, AIAA Paper No, 2000-3969.

Sharma, M., Wise, K., and Lavretsky, E. (2006), 'Application and Flight Testing of an Adaptive Autopilot on Precision Guided Munitions', *Proceedings Of the 2006 AIAA Guidance, Navigation, and Control Conference*, Keystone, CO, AIAA Paper No. 2005-6568.

Steinberg, M. (2005), 'Historical Overview of Research in Reconfigurable Flight Control', *Proceedings of the Institution of Mechanical Engineers. Part G: Journal of Aerospace Engineering*, 219, 263–275.

Urnes-Jr, J.E. (1999), 'NASA F-15 Intelligent Flight Control', *Final Report*, St Louis, MO, Boeing Report No. STL 99P0040.

Ward, D.E. (1998), 'Self Designing Controller', *Final Report*, AFRL WL-TR-97-3095.

Wise, K.A. ''Reconfigurable Systems for Tailless Fighter Aircraft - RESTORE'', Final Report, AFRL-VA–WP-TR-99-3067.

Wise, K.A. (1990), 'Bank-to-turn Missile Autopilot Design using Loop Transfer Recovery', *Journal of Guidance, Control, and Dynamics*, 13, 145–152.

Wise, K.A., and Brinker, J.S. (1996), 'Linear Quadratic Flight Control for Ejection Seats', *Journal of Guidance, Control, and Dynamics*, 19, 15–22.

Wise, K., and Brinker, J. (1998), 'Reconfigurable Flight Control for a Tailless Advanced Fighter Aircraft', *Proceedings of the AIAA GNC Conference*, Boston, MA, pp. 75–87.

Wise, K., Brinker, J., Calise, A., Enns, D., Elgersma, M., and Voulgaris, P. (1999), 'Direct Adaptive Reconfigurable Flight Control for a Tailless Advanced Fighter Aircraft', *International Journal of Robust Nonlinear Control,* Special Issue on Reconfigurable Flight Control, 9, 999–1012.

Wise, K.A., and Deylami, F. (1991), 'Approximating a Linear Quadratic Missile Autopilot Design Using an Output Feedback Projective Control', *Proceedings of the AIAA Guidance, Navigation, and Control Conference*, New Orleans, LA, pp. 114–122. Paper AIAA 91-2613.

Wise, K.A., Lavretsky, E., and Hovakimyan, N. (2006), 'Adaptive Control of Flight: Theory, Applications, and Open Problems', *2006 ACC*, Minneapolis MN, also presented at the *Thirteenth Yale Workshop on Adaptive and Learning Systems*', Connecticut, New Haven.

Wise, K., Lavretsky, E., Zimmerman, J., Francis-Jr, J., Dixon, D., and Whitehead, B. (2005), 'Adaptive Flight Control of a Sensor Guided Munition.', *Proceedings of AIAA Guidance, Navigation and Control Conference*, San Francisco, CA, AIAA Paper No. 2005-6385.